Spin-split bands cause the indirect band gap of (CH₃NH₃)PbI₃: Experimental evidence from circular photogalvanic effect

Daniel Niesner*,¹ Martin Hauck,² Shreetu Shrestha,³ Ievgen

Levchuk,³ Gebhard J. Matt,³ Andres Osvet,³ Miroslaw Batentschuk,³

Christoph Brabec,^{3,4} Heiko B. Weber,² and Thomas Fauster¹

¹ Lehrstuhl für Festkörperphysik, FriedrichAlexander-Universität Erlangen-Nürnberg (FAU),

Staudtstr. 7, 91058 Erlangen, Germany

² Lehrstuhl für Angewandte Physik, FriedrichAlexander-Universität Erlangen-Nürnberg (FAU),

Staudtstr. 7, 91058 Erlangen, Germany

³ Institute of Materials for Electronics and Energy Technology (I-MEET),

Department of Materials Science and Engineering,

Friedrich-Alexander-Universität Erlangen-Nürnberg (FAU),

Martensstrasse 7, 91058 Erlangen, Germany

⁴ Bavarian Center for Applied Energy Research (ZAE Bayern),

Haberstrasse 2a, 91058 Erlangen, Germany

(Dated: November 5, 2021)

Abstract

Long carrier lifetimes and diffusion lengths form the basis for the successful application of the organic-inorganic perovskite (CH₃NH₃)PbI₃ in solar cells and lasers. The mechanism behind the long carrier lifetimes is still not completely understood. Spin-split bands and a resulting indirect band gap have been proposed by theory. Using near band-gap left-handed and right-handed circularly polarized light we induce photocurrents of opposite directions in a single-crystal (CH₃NH₃)PbI₃ device at low temperature (4 K). The phenomenom is known as the circular photogalvanic effect and gives direct evidence for phototransport in spin-split bands. Simultaneous photoluminecence measurements show that the onset of the photocurrent is below the optical band gap. The results prove that an indirect band gap exists in (CH₃NH₃)PbI₃ with broken inversion symmetry as a result of spin-splittings in the band structure. This information is essential for understanding the photophysical properties of organic-inorganic perovskites and finding lead-free alternatives. Furthermore, the optically driven spin currents in (CH₃NH₃)PbI₃ make it a candidate material for spintronics applications.

Organic-inorganic perovskite semiconductors (OIPS) show remarkable potential for applications in highly efficient thin-film solar cells [1–3] and nanolasers [4]. Unusually long carrier lifetimes [5, 6] and diffusion lengths [7, 8] form the basis of their exceptional performance in optoelectronic devices. Strong spin-orbit coupling due to the constituting heavy elements [9–12] and a resulting slightly indirect band gap have been proposed as origin of the observed long carrier lifetimes [13–15]. The direct-indirect character of the band gap of (CH₃NH₃)PbI₃ was recently evidenced experimentally [16, 17]. Direct experimental evidence for spin-orbit coupling as the origin of the indirect band gap, however, is still missing to the best of our knowledge.

To gain insight into the mechanism giving rise to the indirect gap of (CH₃NH₃)PbI₃, we excite photocurrents with left-handed and right-handed circularly polarized light as illustrated in Fig. 1 (a). In the absence of spin-orbit coupling the direction of the excited photocurrent does not depend on the helicity of the incoming light. The spin structure of the electronic band structure causes differences in the optical transition matrix elements as illustrated in Fig. 1 (b). For opposite helicity of the light the group velocity of carriers is reversed and spin-polarized currents of opposite direction are induced [18, 19]. They enhance or reduce the overall photocurrent, respectively. The effect is known as the circular photogalvanic effect. It has been observed experimentally in GaAs/AlGaAs quantum well structures [20], in wurtzite semiconductors such as ZnO [21] and GaN [22], in transition-metal dichalcogenides [23], and in the topological insulator Bi₂Se₃ [24]. A circular photogalvanic effect of measurable magnitude has been predicted [25] for (CH₃NH₃)PbI₃. Previously, circular dichroism has been found in optical [26] and electron spectroscopy [27] experiments on OIPS. A circular photogalvanic effect is hence expected if coherent spin transport takes place on a length scale large enough for spin-polarized currents to be driven through a device.

Results of polarization-dependent photocurrent measurements performed on single-crystal (CH₃NH₃)PbI₃ are shown in Fig. 2 (a) for different excitation photon energies. The sample temperature is 4 K. To control the polarization of the incident light a zero-order $\lambda/4$ plate is introduced in the excitation pathway. The polarizing waveplate is rotated while the photocurrent is measured. The angle of the $\lambda/4$ plate is given along the horizontal axis in Fig. 2 (a). At all wavelengths, a variation of the photocurrent is observed due to changing contributions of p and s-polarized light fields to the excitation. This signal has a periodicity of 90° in the angle of the waveplate. At an angle of $n \cdot 90^{\circ}$ ($n \in \mathbb{N}_0$) the light

is p-polarized and the photocurrent has a minimum. Local maxima occur at 45° (135°), where the light is circularly polarized and the component of s-polarized light is the largest. The variations may result from differences in reflectivity at the surface of the OIPS due to changing contributions of p and s-polarized light, from anisotropies in absorption along the crystalline directions associated with s and p polarization, and from a linear photogalvanic effect [28]. Since differences in the photocurrents excited with s-polarized light and circularly polarized light with p-components can occur in any material and their interpretation is complex, they will not be in the focus of our discussion. However, it is worth noting that a linear photogalvanic effect necessarily goes hand in hand with the circular photogalvanic effect [24, 28].

An additional modulation of the photocurrent induced by the light polarization is clearly observed upon excitation at 1.55 eV and 1.61 eV photon energy. This signal has a periodicity of 180° in the angle of the waveplate, resulting in different photocurrents at $45^{\circ} + n \cdot 180^{\circ}$ and $135^{\circ} + n \cdot 180^{\circ}$. As these angles correspond to left-handed and right-handed circularly polarized light, the differences represent the circular photogalvanic effect. To extract the contribution of the circular photogalvanic effect to the photocurrent, we fit the data with a sum of two cosine functions. The two components are shown individually in Fig. 2 (b). The effect of linear polarization is given by the blue curve. The signal arising from the circular photogalvanic effect, indicated by the red curve, is phase-shifted by 90°. Its contribution to the photocurrent vanishes whenever the light is linearly polarized $(n \cdot 90^{\circ})$. For left-handed (45°) and right-handed (135°) circular polarization, in contrast, it switches sign. The reversal of the photocurrents as the helicity of the excitation light is switched is characteristic for materials with spin-split band structures [20–24]. It implies that spin currents are driven by photoexcitation with circularly polarized light, as indicated in Fig. 1 (b). Light of different helicity couples to opposite branches of the spin-split band structure in k-space. Since the opposite branches do not only carry electrons of opposite spin orientation, but also of reversed group velocity dE/dk, spin-polarized currents are induced along opposite directions. We observe a modification of the overall photocurrent by $\pm 1.5\%$. The amplitude of the circular photogalvanic effect relative to the average photocurrent is given by red symbols in Fig. 3 (a).

The photocurrent (normalized to electrons/photon) is shown as black dots connected by lines to guide the eye in Fig. 3(a). The onset of the photocurrent is well described by a

fourth-power dependence on energy starting at 1.56 ± 0.01 eV. The large exponent can be understood as the result of an indirect band gap in combination with a low density of states of OIPS at the band edges [27, 29]. A small current flows for photon energies below the onset because of the applied bias voltage. Note that the circular photogalvanic effect sets in right at the onset of the photocurrent. The photocurrent reaches its maximum at 1.62 eV photon energy which may be taken as an estimate for the direct band gap. This results in a difference between the direct and indirect gap of 60 ± 15 meV in agreement with literature [16, 17, 30]. The circular photogalvanic effect proves that the spin-orbit coupling of the Rashba effect is responsible for the indirect band gap in $(CH_3NH_3)PbI_3$.

In order to corroborate the assignment of the direct band gap we performed in situ photoluminescence (PL) measurements on the sample at 4 K. A comparison of photocurrent excitation and PL spectra is given in Fig. 3. The low-temperature PL spectrum of $(CH_3NH_3)PbI_3$ consists of a high-energy emission feature at 1.64 ± 0.01 eV, a second peak at 1.61 ± 0.01 eV, and broad low-energy continuum emission with a maximum at 1.56 ± 0.01 eV, in agreement with previous reports [31–34]. The positions of the maxima are indicated by magenta tick marks in Fig. 3(b). Following the literature [32], we assign the highestenergy peak at 1.64 eV to the optical band gap of orthorhombic (CH₃NH₃)PbI₃. The value matches the optical band gap found from magneto-absorption measurements [35]. Emission and absorption at lower photon energies have been attributed to excitons localized at defects [32, 33] and to coexisting structural phases [31, 34]. The assignment of optical transitions to bound or free excitons is difficult based on optical spectroscopy alone. Connecting the PL spectroscopy to the transport measurements at low temperature, we find that currents are generated with photon energies as low as 1.56 eV, demonstrating that free excitons are excited at these photon energies. We attribute the photocurrent to tetragonal [34, 36] and low-symmetry orthorhombic [31] domains coexisting with the lowtemperature, inversion-symmetric orthorhombic phase. The photocurrent has a maximum at 1.62 eV which coincides with the second PL emission peak, indicating an allowed optical transition. We assign the maximum to the direct gap of the tetragonal and low-symmetry orthorhombic domains, in good agreement with the value of 1.61 eV found from magnetoabsorption on tetragonal (CH₃NH₃)PbI₃ [35, 37]. The photocurrent drops by 40% as the photon energy exceeds the optical gap of 1.64 eV of orthorhombic (CH₃NH₃)PbI₃. A smaller photocurrent in orthorhombic (CH₃NH₃)PbI₃ than in the tetragonal phase has been reported before and assigned to less efficient generation of free excitons [16]. Note that the amplitude of the circular photogalvanic effect also drops in the energy range when the inversion symmetric low-temperature orthorhombic phase contributes to the photocurrent.

The observed circular photogalvanic effect unambiguously identifies spin splittings in the band structure as the origin of the indirect gap. A slightly indirect band gap by 47 meV was reported for tetragonal (CH₃NH₃)PbI₃ resulting in an enhanced lifetime of photoexcited carriers as compared to the direct band-gap orthorhombic phase [16]. The lifetime enhancement was found to be absent in the low-temperature orthorhombic phase. While calculations point towards Rashba and Dresselhaus type spin splittings as the origin of the slightly indirect gap [9-12, 17], experimental evidence for this interpretation is, to the best of our knowledge, lacking. Requirements for spin splittings are spin-orbit coupling and absence of inversion symmetry. It is worth noting that Rashba and Dresselhaus spin splittings are caused by the local environment of the atoms in the unit cell rather than by the average, long-range symmetry of the crystal [38]. A Rashba-type spin-split band structure was found in the valence band at the surface of related (CH₃NH₃)PbBr₃ perovskite using angleresolved photoelectron spectroscopy [27]. Surfaces break inversion symmetry inherently and enhance Rashba splitting. Observation of the circular photogalvanic effect demonstrates that spin-splittings occur in the bulk of (CH₃NH₃)PbI₃ on a length scale relevant for carrier transport. We find a stronger effect at low photon energies than for higher ones. The corresponding transitions can be assigned to tetragonal and low-symmetry orthorhombic domains (< 1.64 eV) and to the inversion symmetric low-temperature orthorhombic phase $(\geq 1.64 \text{ eV})$, respectively. For the latter, a prominent photogalvanic effect is not expected. The former, in contrast, has a locally broken inversion symmetry at all temperatures [39, 40]. The spin splittings in the band structure observed here at 4 K are hence expected to persist for temperatures up to room temperature, as implied also by the strong circular dichroism found in optical spectroscopy at room temperature [26].

The observed difference between the optical and the transport gap of 60 ± 15 meV of tetragonal (CH₃NH₃)PbI₃ is large enough to pose an energetic barrier for electron-hole-pair recombination even at room temperature. Activation energies of 75 meV [30] and 47 meV [16] for radiative recombination were reported previously, in good agreement with our results. Calculations find a value of 75 meV as a result of spin-splittings in the band structure of (CH₃NH₃)PbI₃ [15]. They predict an increasing splitting with increasing temperature, in

agreement with optical spectroscopic results obtained from related (CH₃NH₃)PbBr₃ single crystals [41].

Our results clarify the mechanism behind the indirect character of the band gap of $(CH_3NH_3)PbI_3$. This helps to understand the excellent performance of OIPS in optoelectronic devices and provides a design rule for less toxic alternatives to $(CH_3NH_3)PbI_3$. Lifetime enhancements by a factor of 10 to 350 have been predicted as the result of Rashba-type spin splitting restricting optical transitions [13–15], making it an essential ingredient to the observed long carrier diffusion lengths. [16]

Spin splittings of this magnitude do not only enhance carrier lifetimes. They also allow to optically drive spin currents [42–44] in the system. The spin splitting of 60 ± 15 meV is similar to the strongest ones found in known bulk Rashba systems, such as BiTeX (X = Cl [45], Br [46], I [47]) and GeTe(111) [48]. In contrast to these materials, (CH₃NH₃)PbI₃ has a band gap in the near-infrared range making it a candidate material for opto-spintronics applications [43]. Additional applications become possible if structures with a switchable ferroelectric polarization can be grown [49, 50], as they have been found at the surface of (CH₃NH₃)PbI₃ [51], where the Rashba splitting in organic-inorganic perovskite is further enhanced [27].

We find a measurable circular photogalvanic effect of $\pm 1.5\%$ in rather large devices with a channel width of 1 mm. Significant spin currents can be expected when device dimensions are reduced to the spin transport length. From magneto-transport and magneto-optical experiments, a spin-lattice relaxation time τ of 200 ps was estimated for spin-cast (CH₃NH₃)PbI₃ thin films [52]. Carrier diffusion coefficients in (CH₃NH₃)PbI₃ thin films are around $D = 0.05 \text{ cm}^2\text{s}^{-1}$ [7, 53], translating into a spin diffusion length $l = \sqrt{D \cdot \tau} = 30 \text{ nm}$. The carrier diffusion constant in single crystals is larger than in thin films by a factor of ≈ 20 [8, 53, 54], and also the spin relaxation time can be expected to be enhanced. Spin diffusion lengths of hundreds of nanometers may hence be achieved in OIPC single crystals.

ACKNOWLEDGEMENTS

I. L., A. O., S. S., M. B., and C. J. B. gratefully acknowledge financial support from the Soltech Initiative, the Excellence Cluster "Engineering of Advanced Materials" (EAM) granted to the University Erlangen-Nuremberg, and from the Energiecampus Nürnberg. Funding from the Emerging Fields initiative "Singlet Fission" supported by Friedrich-Alexander-Universität Erlangen-Nürnberg is gratefully acknowledged by D. N., M. W., and T. F.

METHODS

Device fabrication. (CH₃NH₃)PbI₃ single crystals were grown by the seed-solution growth method following the procedure described in Ref. [55]. Crystals were prepared and kept under N₂ atmosphere before they got contacted with 40 nm of gold at a spacing of 1 mm. Contacts are aligned with the macroscopic facets of the crystals. The crystals are mounted under ambient conditions (exposure for ≈ 2 h) in a vacuum cryostat. Immediately after pumping the cryostat, crystals are cooled to 4 K. Keeping the crystals in vacuum at room temperature for extended periods of time (> 12 h) results in changes in the spectra, whereas no changes are observed for the cooled crystals under prolonged (4 h) illumination with laser light, see Fig. S1 in Supplementary Information. We demonstrated that methylamine desorbs from (CH₃NH₃)PbBr₃ in vacuum just above room temperature [27] and speculatively assign the degradation of (CH₃NH₃)PbI₃ to the same mechanism.

Photocurrent and photoluminescence measurements. Photocurrents are excited with a Ti:Sa laser in cw mode. Laser powers are around 3 mW with a Gaussian spot radius of 0.3 mm. The voltage applied to the device is swept between -0.5 V and +0.5 V to avoid slow changes [56, 57] in the structure of $(CH_3NH_3)PbI_3$. No hysteresis is observed in the I(V) sweeps, see Fig. S2 in Supplementary Information. The data are shown for a small bias voltage (0.25 V). Results presented here are independent of the applied bias voltage for 0 < |V| < 0.5 V except for the amplitude of the measured photocurrents. Photocurrents are normalized to the number of incident photons to account for variations in the laser power at different photon energies. The photocurrent increases linearly with excitation density as shown in Fig. S3 in Supplementary Information.

For photoluminescence experiments the channel of the (CH₃NH₃)PbI₃ device was optically excited with a 532 nm cw laser between photocurrent measurementss. The PL spectra were recorded using an Ocean Optics HR 4000 spectrometer. A dielectric long pass filter (550 nm) was used to suppress scattered light from the illuminated surface from which the

- [1] Yang, W. S. *et al.* High-performance photovoltaic perovskite layers fabricated through intramolecular exchange. *Science* **348**, 1234–1237 (2015).
- [2] Saliba, M. et al. A molecularly engineered hole-transporting material for efficient perovskite solar cells. Nat. Energy 1, 15017 (2016).
- [3] Stranks, S. D. & Snaith, H. J. Metal-halide perovskites for photovoltaic and light-emitting devices. *Nat. Nanotechnol.* **10**, 391–402 (2015).
- [4] Zhu, H. et al. Lead halide perovskite nanowire lasers with low lasing thresholds and high quality factors. Nat. Mater. 14, 636–642 (2015).
- [5] Bi, Y. et al. Charge Carrier Lifetimes Exceeding 15 μs in Methylammonium Lead Iodide Single Crystals. J. Phys. Chem. Lett. 7, 923 (2016).
- [6] Xu, W. et al. Iodomethane-Mediated Organometal Halide Perovskite with Record Photoluminescence Lifetime. ACS Appl. Mater. Interfaces 8, 23181–23189 (2016).
- [7] Stranks, S. D. *et al.* Electron-hole diffusion lengths exceeding 1 micrometer in an organometal trihalide perovskite absorber. *Science* **342**, 341–344 (2013).
- [8] Dong, Q. et al. Electron-hole diffusion lengths > 175 μ m in solution-grown CH₃NH₃PbI₃ single crystals. Science **347**, 967 (2015).
- [9] Even, J., Pedesseau, L., Jancu, J.-M. & Katan, C. Importance of spin-orbit coupling in hybrid organic/inorganic perovskites for photovoltaic applications. J. Phys. Chem. Lett. 4, 2999 (2013).
- [10] Brivio, F., Butler, K. T., Walsh, A. & van Schilfgaarde, M. Relativistic quasiparticle self-consistent electronic structure of hybrid halide perovskite photovoltaic absorbers. *Phys. Rev. B* 89, 155204 (2014).
- [11] Quarti, C., Mosconi, E. & De Angelis, F. Interplay of Orientational Order and Electronic Structure in Methylammonium Lead Iodide: Implications for Solar Cell Operation. *Chem. Mater.* 26, 6557–6569 (2014).
- [12] Demchenko, D. et al. Optical properties of the organic-inorganic hybrid perovskite CH₃NH₃PbI₃: Theory and experiment. Phys. Rev. B **94**, 075206 (2016).
- [13] Zheng, F., Tan, L. Z., Liu, S. & Rappe, A. M. Rashba Spin-Orbit Coupling Enhanced Carrier

- Lifetime in CH₃NH₃PbI₃. Nano Lett. **15**, 7794–7800 (2015).
- [14] Etienne, T., Mosconi, E. & De Angelis, F. Dynamical Origin of the Rashba Effect in Organohalide Lead Perovskites: A Key to Suppressed Carrier Recombination in Perovskite Solar Cells? J. Phys. Chem. Lett. 7, 1638 (2016).
- [15] Azarhoosh, P., McKechnie, S., Frost, J. M., Walsh, A. & van Schilfgaarde, M. Research Update: Relativistic origin of slow electron-hole recombination in hybrid halide perovskite solar cells. APL Mater. 4, 091501 (2016).
- [16] Hutter, E. M. et al. Direct-indirect character of the bandgap in methylammonium lead iodide perovskite. Nat. Mater. 16, 115 (2016).
- [17] Wang, T. et al. Indirect to direct bandgap transition in methylammonium lead halide perovskite. Energy Environ. Sci. 10, 509 (2017).
- [18] Belinicher, V. Space-oscillating photocurrent in crystals without symmetry center. Phys. Lett. A 66, 213–214 (1978).
- [19] Ganichev, S. D. & Golub, L. E. Interplay of Rashba/Dresselhaus spin splittings probed by photogalvanic spectroscopy—A review. *Phys. Status Solidi* (b) **251**, 1801–1823 (2014).
- [20] Lechner, V. et al. Spin and orbital mechanisms of the magnetogyrotropic photogalvanic effects in $GaAs/Al_x Ga_{1-x}$ As quantum well structures. Phys. Rev. B 83, 155313 (2011).
- [21] Zhang, Q. et al. Strong circular photogalvanic effect in ZnO epitaxial films. Appl. Phys. Lett. 97, 041907 (2010).
- [22] Weber, W. et al. Demonstration of Rashba spin splitting in GaN-based heterostructures.

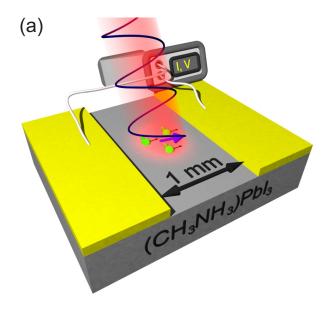
 Appl. Phys. Lett. 87, 262106 (2005).
- [23] Yuan, H. et al. Generation and electric control of spin-valley-coupled circular photogalvanic current in WSe₂. Nat. Nanotechnol. 9, 851–857 (2014).
- [24] McIver, J., Hsieh, D., Steinberg, H., Jarillo-Herrero, P. & Gedik, N. Control over topological insulator photocurrents with light polarization. *Nat. Nanotechnol.* **7**, 96–100 (2012).
- [25] Li, J. & Haney, P. M. Circular photogalvanic effect in organometal halide perovskite CH₃NH₃PbI₃. Appl. Phys. Lett. **109**, 193903 (2016).
- [26] Giovanni, D. *et al.* Highly spin-polarized carrier dynamics and ultralarge photoinduced magnetization in CH₃NH₃PbI₃ perovskite thin films. *Nano Lett.* **15**, 1553 (2015).
- [27] Niesner, D. et al. Giant Rashba Splitting in CH₃NH₃PbBr₃ Organic-Inorganic Perovskite. Phys. Rev. Lett. 117, 126401 (2016).

- [28] Ganichev, S. D. & Prettl, W. Spin photocurrents in quantum well structures. *J. Phys. Condens. Matter* **15**, R935 (2003).
- [29] Endres, J. et al. Valence and Conduction Band Densities of States of Metal Halide Perovskites: A Combined Experimental-Theoretical Study. J. Phys. Chem. Lett. 7, 2722 (2016).
- [30] Savenije, T. J. et al. Thermally activated exciton dissociation and recombination control the carrier dynamics in organometal halide perovskite. J. Phys. Chem. Lett. 5, 2189–2194 (2014).
- [31] Dar, M. I. et al. Origin of unusual bandgap shift and dual emission in organic-inorganic lead halide perovskites. Sci. Adv. 2, e1601156 (2016).
- [32] Diab, H. et al. Narrow Linewidth Excitonic Emission in Organic-Inorganic Lead Iodide Perovskite Single Crystals. J. Phys. Chem. Lett. 7, 5093–5100 (2016).
- [33] Wu, X. et al. Trap states in lead iodide perovskites. J. Am. Chem. Soc. 137, 2089–2096 (2015).
- [34] Galkowski, K. et al. Spatially resolved studies of the phases and morphology of methylammonium and formamidinium lead tri-halide perovskites. Nanoscale 9, 3222 (2017).
- [35] Miyata, A. et al. Direct measurement of the exciton binding energy and effective masses for charge carriers in organic-inorganic tri-halide perovskites. Nat. Phys. 11, 582 (2015).
- [36] Phuong, L. Q. et al. Free Carriers Versus Excitons in CH₃NH₃PbI₃ Perovskite Thin Films at Low Temperatures: Charge Transfer From the Orthorhombic Phase to the Tetragonal Phase.

 J. Phys. Chem. Lett. 7, 2316 (2016).
- [37] Galkowski, K. et al. Determination of the exciton binding energy and effective masses for methylammonium and formamidinium lead tri-halide perovskite semiconductors. Energy Environ. Sci., 9, 962 (2016).
- [38] Zhang, X., Liu, Q., Luo, J.-W., Freeman, A. J. & Zunger, A. Hidden spin polarization in inversion-symmetric bulk crystals. *Nat. Phys.* 10, 387–393 (2014).
- [39] Druźbicki, K. et al. Unexpected Cation Dynamics in the Low-Temperature Phase of Methylammonium Lead Iodide: The Need for Improved Models. J. Phys. Chem. Lett. 7, 4701–4709 (2016).
- [40] Beecher, A. N. et al. Direct Observation of Dynamic Symmetry Breaking above Room Temperature in Methylammonium Lead Iodide Perovskite. ACS Energy Lett. 1, 880–887 (2016).
- [41] Niesner, D. et al. Temperature-dependent optical spectra of single-crystal CH₃NH₃PbBr₃ cleaved in ultrahigh vacuum. Phys. Rev. B **95**, 075207 (2017).

- [42] Kepenekian, M. et al. Rashba and Dresselhaus Effects in Hybrid Organic–Inorganic Perovskites: From Basics to Devices. ACS Nano 9, 11557 (2015).
- [43] Li, J. & Haney, P. M. Optical spintronics in organic-inorganic perovskite photovoltaics. Phys. Rev. B 93, 155432 (2016).
- [44] Zhang, C., Sun, D. & Vardeny, Z. V. Multifunctional optoelectronic–spintronic device based on hybrid organometal trihalide perovskites. *Adv. Electron. Mater.* **3** (2017).
- [45] Landolt, G. et al. Bulk and surface Rashba splitting in single termination BiTeCl. New J. Phys. 15, 085022 (2013).
- [46] Ogawa, N., Bahramy, M., Kaneko, Y. & Tokura, Y. Photocontrol of Dirac electrons in a bulk Rashba semiconductor. Phys. Rev. B 90, 125122 (2014).
- [47] Ishizaka, K. et al. Giant Rashba-type spin splitting in bulk BiTeI. Nat. Mater. 10, 521 (2011).
- [48] Liebmann, M. et al. Giant Rashba-Type Spin Splitting in Ferroelectric GeTe (111). Adv. Mater. 28, 560–565 (2016).
- [49] Kim, M., Im, J., Freeman, A. J., Ihm, J. & Jin, H. Switchable S= 1/2 and J= 1/2 Rashba bands in ferroelectric halide perovskites. *Proc. Natl. Acad. Sci.* 111, 6900 (2014).
- [50] Leppert, L., Reyes-Lillo, S. E. & Neaton, J. B. Electric Field-and Strain-Induced Rashba Effect in Hybrid Halide Perovskites. J. Phys. Chem. Lett. 7, 3683–3689 (2016).
- [51] Kutes, Y. et al. Direct Observation of Ferroelectric Domains in Solution-Processed CH₃NH₃PbI₃ Perovskite Thin Films. J. Phys. Chem. Lett. **5**, 3335 (2014).
- [52] Zhang, C. et al. Magnetic field effects in hybrid perovskite devices. Nat. Phys. 11, 427–434 (2015).
- [53] Guo, Z., Manser, J. S., Wan, Y., Kamat, P. V. & Huang, L. Spatial and temporal imaging of long-range charge transport in perovskite thin films by ultrafast microscopy. *Nat. Commun.* 6, 7471 (2015).
- [54] Shi, D. et al. Low trap-state density and long carrier diffusion in organolead trihalide perovskite single crystals. Science **347**, 519–522 (2015).
- [55] Zhou, Y. et al. Giant photostriction in organic-inorganic lead halide perovskites. Nat. Commun. 7, 11193 (2016).
- [56] Gottesman, R. et al. Extremely slow photoconductivity response of CH₃NH₃PbI₃ perovskites suggesting structural changes under working conditions. J. Phys. Chem. Lett. 5, 2662–2669 (2014).

[57] Gottesman, R. et al. Photoinduced reversible structural transformations in free-standing CH₃NH₃PbI₃ perovskite films. J. Phys. Chem. Lett. **6**, 2332–2338 (2015).



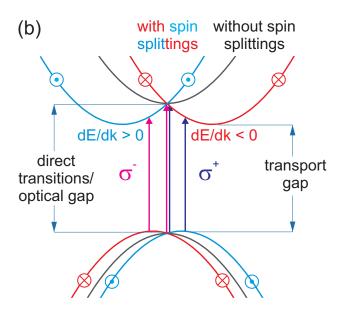


Figure 1. Circular photogalvanic effect: Experimental setup and schematic illustration in momentum space. (a) The (CH₃NH₃)PbI₃ single crystal with gold contacts (channel width: 1 mm) is illuminated by monochromatic cw light of tunable photon energy close to the band gap. The angle of incidence is 31° with respect to the surface normal. (b) Rashba and Dresselhaustype spin splittings lift the spin-degeneracy of electronic bands. Excitation with left- (σ^-) and right-handed (σ^+) circularly polarized light creates photocarriers on opposite branches of the band structure. Since the associated group velocities dE/dk differ, a spin current is induced as indicated in (a).

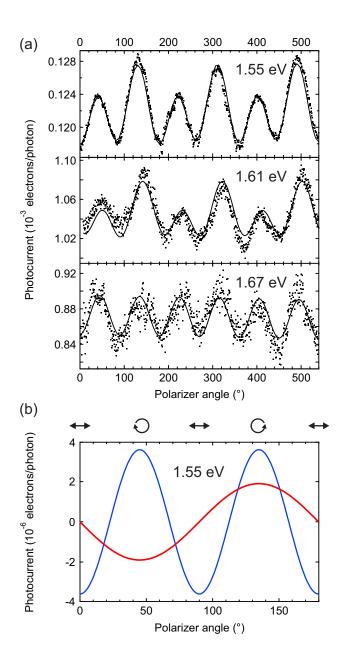


Figure 2. Polarization dependence of photocurrent. (a) The photocurrent induced with laser light of photon energies (1.55 eV and 1.61 eV) below the band gap (1.64 eV) shows a periodicity of 180° with respect to the angle of the $\lambda/4$ waveplate, which changes to 90° for above band gap excitation (1.67 eV). Photocurrents are normalized to the incoming photon flux. (b) shows results of a fit to the data in (a). The phase shift between the cosine components with 90° periodicity (red) and 180° periodicity (blue) is 90°. The latter hence represents a circular photogalvanic signal with opposite directions of the currents induced by left-handed and right-handed circularly polarized light.

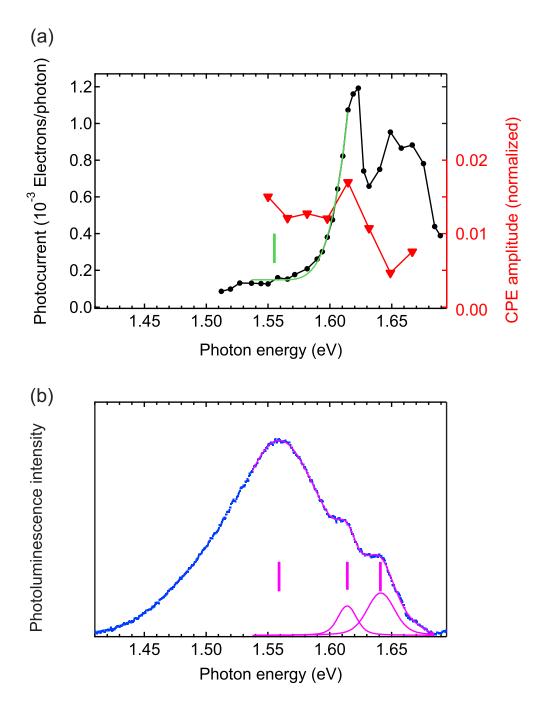


Figure 3. Transport gap and optical gap of (CH₃NH₃)PbI₃. (a) Photocurrent excited by monochromatic laser light (black symbols). The onset of the photocurrent (tick mark) is extracted by a power law fit (green curve) yielding a fourth power dependence. The amplitude of the circular photogalvanic effect (CPE amplitude) normalized to the average photocurrent extracted from Fig. 2 (a) is shown by red symbols. The data points are connected for clarity. (b) The photoluminescence spectrum (blue symbols) is fitted (magenta) by a sum of three Voigtian peaks. Peak positions are given by tick marks.